# We are IntechOpen,
# the world's leading publisher of
# Open Access books
# Built by scientists, for scientists

## 4,800
Open access books available

## 122,000
International authors and editors

## 135M
Downloads

Our authors are among the

## 154
Countries delivered to

## TOP 1%
most cited scientists

## 12.2%
Contributors from top 500 universities

**BOOK CITATION INDEX**
CLARIVATE ANALYTICS
INDEXED

**WEB OF SCIENCE**™

Selection of our books indexed in the Book Citation Index
in Web of Science™ Core Collection (BKCI)

## Interested in publishing with us?
## Contact book.department@intechopen.com

Numbers displayed above are based on latest data collected.
For more information visit www.intechopen.com

# A Review of Wind Turbine Yaw Aerodynamics

Daniel Micallef and Tonio Sant

Additional information is available at the end of the chapter

**Abstract**

The fundamental physics of HAWT aerodynamics in yaw is reviewed with reference to some of the latest scientific research covering both measurements and numerical modelling. The purpose of this chapter is to enable a concise overview of this important subject in rotor aerodynamics. This will provide the student, researcher or industry professional a quick reference. Detailed references are included for those who need to delve deeper into the subject. The chapter is also restricted to the aerodynamics of single rotors and their wake characteristics. Far wake and wind turbine to turbine effects experienced in wind farms are excluded from this review. Finally, a future outlook is provided in order to inspire further research in yawed aerodynamics.

**Keywords:** horizontal axis wind turbine, yaw, unsteady aerodynamics, wakes, rotors

## 1. Introduction: The relevance of wind turbine yaw aerodynamics

### 1.1. Wind turbine yaw fundamentals

A wind turbine converts the kinetic energy from the wind to electrical energy. The power which can be extracted is proportional to the cube of the wind speed. There is, however, a theoretical limit to the power which can be extracted from the turbine. This is known as the Betz limit. This limit was derived by Betz [1] to correspond to 59% of the maximum available power which can be extracted by the turbine. The efficiency of a wind turbine is called the power coefficient and is defined by the following:

$$C_P = \frac{P}{\frac{1}{2}\rho U_\infty^3 A}$$

(1)

where $P$ is the turbine power, $\rho$ is the density, $U_\infty$ is the wind velocity and $A$ is the rotor area. In practice, due to various practical reasons, only a fraction of the Betz limit can be exploited. Some reasons for this reduction in the overall efficiency of the turbines are mostly associated with the wind resource itself and include wind shear [2, 3], wind turbulence [4, 5], and yaw. In this chapter, we focus our attention on the latter for the case of a horizontal axis wind turbine (HAWT).

Yaw occurs when the wind direction is not perpendicular to the rotor plane. When the HAWT operates in yaw, the average power extracted by the turbine reduces as compared to the case when the wind is perpendicular to the rotor plane. This yawed flow situation is depicted in **Figure 1** where $\gamma$ is the yaw angle. The blade will experience a varying relative velocity and angle of attack with azimuthal blade position, leading to an unsteady aerodynamics problem.
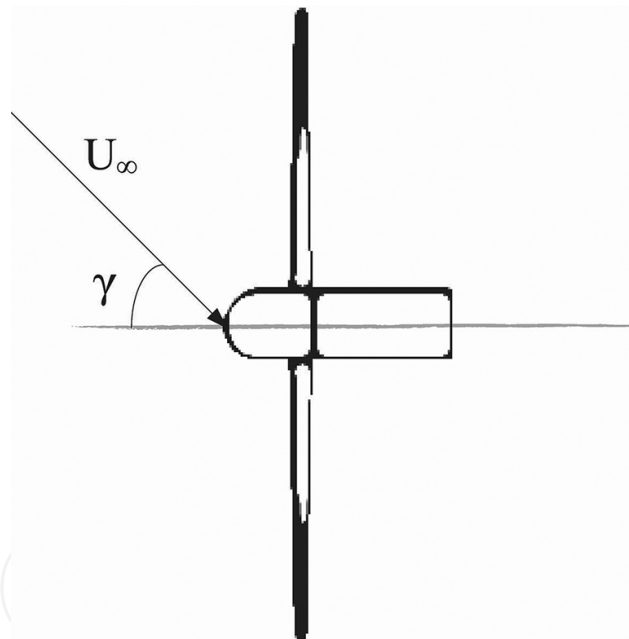


**Figure 1.** Wind turbine operating in yaw.

## 1.2. Relevance of studying yawed flows

Although modern wind turbines allow for various yaw mechanisms in order to align the turbine with respect to the incoming wind, the response to variations in wind direction is very slow. Consequently, the turbine will be in yaw during most of its operational time. Eggleston and Starcher [6] and Madsen et al. [7] show time series results of wind direction as observed from a sensor installed on two different experimental turbines in the field. A time series for

the wind yaw angle measured from the experimental turbines is shown in **Figure 2**. For the Tellus turbine (right figure), during a particular instant in time, the yaw angle increases and varies dramatically. The yaw angle can reach up to around 60°, depending on the wind flow characteristic on site.

While the yawed flow scenario presents an important and challenging problem, the basis of understanding the wind turbine aerodynamics is the axial flow case. The major challenges in the understanding of wind turbine flows are associated with the root and tip flows [8–10]. For an in-depth review of wind turbine aerodynamics, particularly for wind turbines operating in axial flow, the reader is referred to [11] and lately in [12].
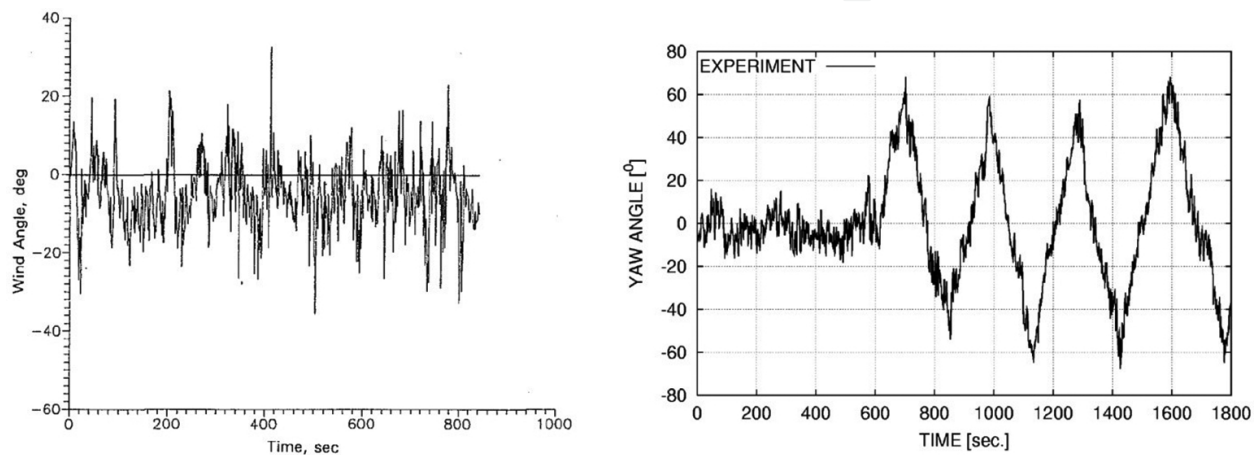


**Figure 2.** Time series of yaw angle during testing of (left) the Carter 25 turbine (wind direction sensor behind nacelle) [6] and (right) the Tellus turbine [7].

Unsteady aerodynamics inevitably results in unsteady loads which negatively affect the power quality and fatigue lifetime of wind turbines. Reference [13] provides a detailed overview of the various challenges in modelling wind turbines under unsteady conditions, including rotor yaw, given the lack of understanding of many aerodynamic phenomena associated with the wake structure developed behind the turbine and the dynamics of unsteady flows over the blade sections.

Wind turbines operating in wind farms are well known to suffer from significant aerodynamic interference losses, primarily due to the axial velocity deficit incurred by the wind flowing through the upstream turbines. The power output from full-scale turbines operating in large wind farms may be as low as 40% of a stand-alone turbine, depending on the turbine spacing as well as environmental flow conditions including the mean wind speed, turbulence intensity and atmospheric stability (see [14]). Yaw aerodynamics may eventually become more important for large offshore wind farm design, given the possibility of mitigating such wake losses by skewing the upstream turbine wake using smart rotor yaw control.

In this chapter, a review of the physics of HAWT aerodynamics in yaw is given by focusing on the aerodynamic phenomena of the near wake and the flow over the rotating blade sections. Far wake and turbine-to-turbine interference effects are excluded from this study. Further-

more, emphasis is made on single HAWT rotors operating in fixed yaw and under steady and uniform wind fronts. Reference is made to some of the latest scientific research in the field, including state-of-the-art wind tunnel measurements undertaken on model turbines under controlled conditions.

## 2. The blade element momentum (BEM) theory

The momentum conservation principle can be applied in order to be able to determine the wake inductions, and hence, the turbine blade loading and performance. In the blade element momentum (BEM) method, the blade is divided into a number of 2D elements. The momentum principle is then applied on aerodynamically independent annular elements. In doing so, a number of limitations and assumptions arise:

a.    Inviscid flow.

b.    Annular air elements are independent (no radial flow from one element to the next).

c.    Aerofoil polars are generally based on 2D wind tunnel measurements.

d.    The loading of the blades on the air is assumed not to vary with azimuth meaning that an infinite number of blades assumed. This must be resolved using tip loss correction methods.

e.    The theory alone cannot be used for highly loaded rotors, where turbulent mixing is prevalent.

The velocity diagram for a particular blade element is shown in **Figure 3**. The relative velocity is given by the following:

$$V_{rel} = \sqrt{\left(U_\infty + V_{axial,ind}\right)^2 + \left(r + V_{\theta,ind}\right)^2} \tag{2}$$

where $V_{axial,ind}$ is the axial wake-induced velocity (which would be opposing the freestream velocity), and $V_{\theta,ind}$ is the tangential wake-induced velocity. The inflow angle $\phi$ (indicated in **Figure 3**) can thus be found from:

$$tan\varphi = \frac{U_\infty + V_{axial,ind}}{r\Omega + V_{\theta,ind}} \tag{3}$$

from which the angle of attack becomes the difference between the inflow angle and the blade's pitch and twist angles (the sum of which is here represented by $\theta$).
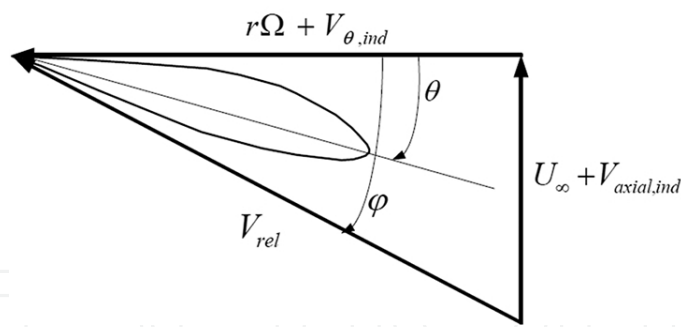
**Figure 3.** Velocity diagram for a blade section in axial flow at radius r. The blade section shown moves from left to right of the figure. Source: Micallef [19].

$$\propto = \varphi - \theta \tag{4}$$

From the aerofoil data, the normal and tangential force coefficients (with respect to the rotor plane) can be determined from the lift and drag coefficients ($C_l$ and $C_d$) and the inflow angle $\phi$ as follows:

$$C_n = C_l cos\varphi + C_d sin\varphi \tag{5}$$

$$C_t = C_l sin\varphi - C_d cos\varphi \tag{6}$$

The induction factors defined as $a_1 = V_{axial,ind}/U_\infty$ and $a_2 = V_{\theta,ind}/r\Omega$ may then be determined applying the law of conservation of momentum in the axial and azimuthal directions by assuming that the momentum expressions are equal to the blade element expressions:

$$4a_1\left(1 - a_1\right)U_\infty^2 = \sigma V_{rel}^2 C_n \tag{7}$$

$$4a_2\left(1 - a_1\right)\Omega r U_\infty r = \sigma V_{rel}^2 C_t r \tag{8}$$

where $a_1$ and $a_2$ are the axial and tangential induction factors. $\sigma$ is defined as the rotor local solidity:

$$\sigma = \frac{Bc}{2\pi r} \tag{9}$$

where $c$ is the chord and $B$ is the number of blades. This formulation does not include the effect of the finite number of blades. The most commonly used approach to deal with this problem

is to use the Prandtl tip loss factor reported [1]. In this formulation, Prandtl uses a disc representation to represent the wake effect and the finite number of blades. This is shown in **Figure 4**.
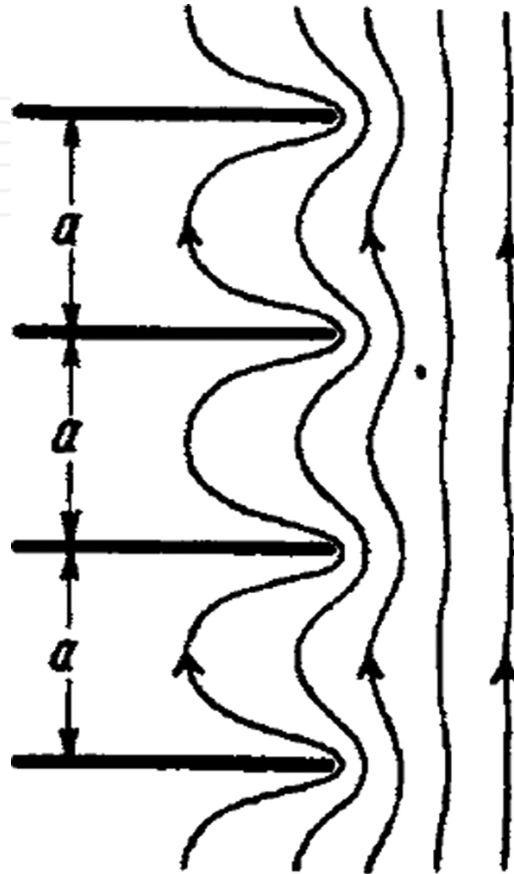


**Figure 4.** Prandtl tip loss model using a number of vorticity discs spaced apart by a distance a. Source: [1].

Prandtl came up with an analytical and implementable solution from a tip loss factor $F$ of the following form:

$$F = \frac{2}{\pi} cos^{-1} \left( exp \left( -\frac{B(R-r)}{2R} \frac{\sqrt{(R)^2 + U_\infty^2 (1-a_1)^2}}{U_\infty (1-a_1)} \right) \right) \tag{10}$$

One way to account for tip loss is to modify Eqs. (13) and (14) to include the tip loss factor and re-arrange them for an iterative solution, as follows:

$$a_1 = \frac{1}{\frac{4F sin^2 \varphi}{\sigma C_n} + 1} \tag{11}$$

$$a_2 = \cfrac{1}{\cfrac{4F sin\varphi cos\varphi}{\sigma C_t} - 1} \tag{12}$$

Various authors, such as in [15], assessed the validity of this model using a computational fluid dynamics (CFD) approach. While the accuracy of the Prandtl tip loss model is debatable, it nonetheless provides a simple solution to a complex problem and is still to date the most common method for accounting for a finite number of blades.

The algorithm for implementing the BEM theory can be found in various textbooks including [15–18]. Here, the one given in [19] is adapted:

1.  Set $a_1 = a_2 = 0$.

2.  Find the flow angle $\phi$ and hence the angle of attack $\alpha$.

3.  Calculate the tip loss factor from Eq. (10).

4.  Read $C_l$ and $C_d$ from the 2D aerofoil polars.

5.  The normal and tangential thrust coefficients $C_n$ and $C_t$ can be calculated from Eqs. (5) and (6).

6.  New values for $a_1$ and $a_2$ can be established from Eqs. (17) and (18).

7.  If $a_1$ and $a_2$ have converged below a defined tolerance, then move to the next step. Otherwise, repeat starting from step 2.

8.  Compute the thrust and torque for the wind turbine rotor using the following:

$$T = B \int_{R_r}^{R} 4\pi\rho U_\infty^2 a_1 (1 - a_1) r \, dr \tag{13}$$

$$Q = B \int_{R_r}^{R} 4\pi\rho U_\infty \, r a_2 (1 - a_1) r^2 \, dr \tag{14}$$

## 3. The BEM theory for yawed wind turbines

### 3.1. Modifications to the axial momentum theory

The linear momentum theory is modified for yawed wind turbines on the basis of Glauert's autogyro theory (see Glauert [20]). Only the normal wind flow component $U_\infty \cos \gamma$ is assumed to be affected by the presence of the actuator disc. It is assumed that this component changes to $U_\infty \cos \gamma + u$ at the disc and the resultant flow velocity here becomes

$$u' = \sqrt{U_\infty{}^2 sin^2\gamma + U_\infty{}^2 \left(cos\gamma - a\right)^2} \tag{15}$$

Glauert expresses the momentum equation for the axial thrust $T$ on the rotor as

$$T = 2\rho A a U_\infty u' \tag{16}$$

The thrust parallel to the plane of the disc is zero as it is assumed that the flow component $U_\infty sin\gamma$ is left unperturbed by the rotor.

In yawed conditions, the wind speed and inflow relative to the moving blades change with azimuth angle. The velocity diagram for the blade at the top-most position is shown in **Figure 5**. The resultant velocities would hence be the following:

$$V_{axial} = U_\infty \cos\gamma - V_{axial,ind} \tag{17}$$

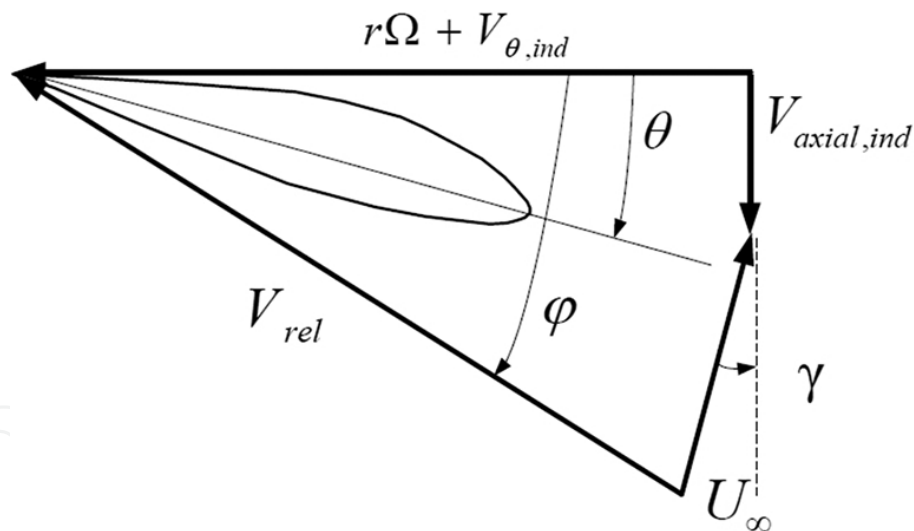$$V_\theta = r\Omega + V_{\theta,ind} - U_\infty sin\gamma \cos\phi \tag{18}$$



**Figure 5.** Velocity diagram for a blade section of a yawed rotor blade at radius r. The blade section is shown at the top most position and rotating clockwise. Source: [39].

Anderson showed, using a BEM approach that the power coefficient of a yawed turbine reduces with increasing yaw [16]. This hypothesis was later confirmed in [17, 18]. The results obtained by [18] for a 2- and 3-bladed rotor are compared with those found in [16, 17] in **Figure 6**. $C_P$ is the power coefficient at a given yaw angle, while $C_{Pmax}$ is that under axial conditions. The rotors which were used in these studies are different, and hence, a qualitative agreement was only obtained.
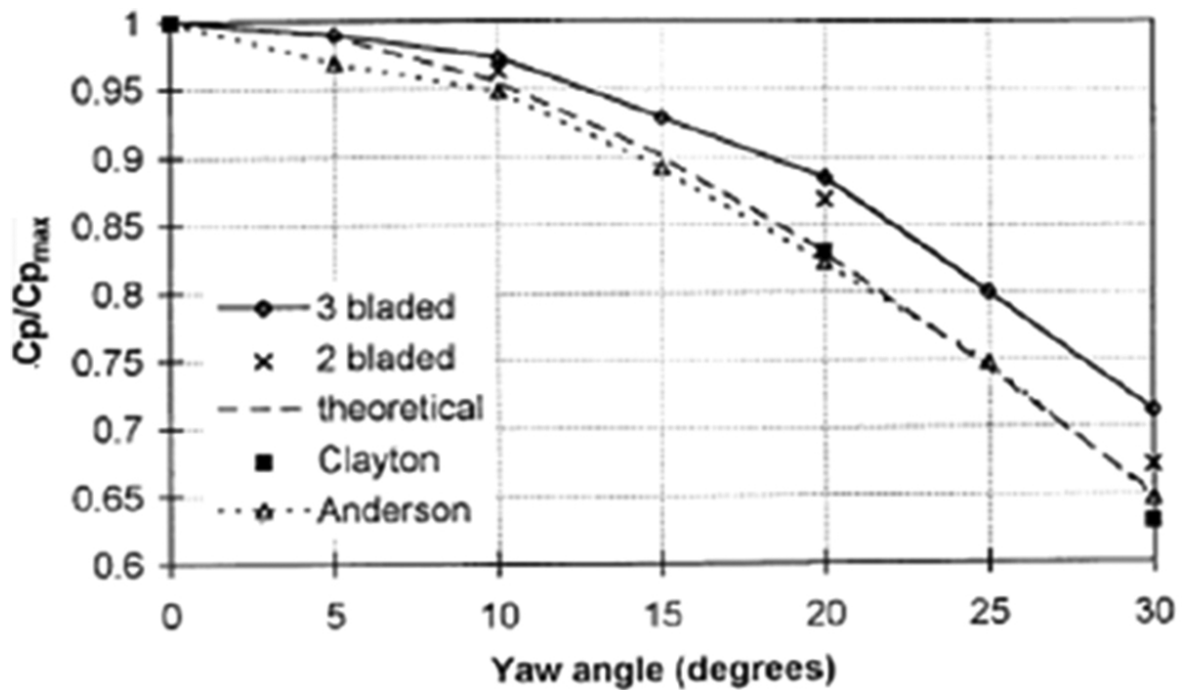
**Figure 6.** Power coefficient normalized by the maximum power coefficient (zero yaw) against yaw angle. Clayton and Filby considered a 3-bladed rotor while Anderson considered a 2-bladed rotor in his BEM analysis. The difference in results is primarily due to the different rotor geometries. The results, however, agree qualitatively (see [18]).

The ratio $C_P/C_{Pmax}$ representing the loss in power due to rotor yaw may be approximated to $\cos^x(\gamma)$. The exponent $x$ is often thought to be equal to 3; however, this is only valid if the axial induction distribution is small compared to $U_\infty \cos \gamma$ or the axial induction factor distribution is unchanged as a result of yaw. Recent wind tunnel measurements on the 0.9 m diameter 3-bladed model at NTNU have shown that the $C_P/C_{Pmax}$ followed well the $\cos^3(\gamma)$ relation (see [21]). A different situation was observed in another measurement. In [22], it is reported that measurements involving both wind tunnel models and full-scale turbines tested at Vattenfall/ FFA and DNW have indicated that the exponent $x$ may vary between 1.8 and 5 for the NREL Phase VI rotor (see [23] pp. 181–183). Such studies have also consistently shown that the BEM theory over predicts the power at yawed conditions. This is possibly related to the limitations of the linear momentum equation modified for yawed flows [Eq. (16)].

Although yawed flow contradicts the fundamental assumption used in BEM of having radially independent annular elements, BEM models have still been used in yaw (refer to [24]). In order to correct for the asymmetric wake induction, a model was first developed in [25] in his work on the autogyro. Ignoring this correction will result in a zero restoring yawing moment, which has been shown experimentally to be unrealistic. Glauert proposed that the induction factor at the blades would take the following form:

$$a = a_1 \left( 1 + K \frac{r}{R} \sin\phi \right) \tag{19}$$

where $a_1$ is the average induction factor, $K$ is a function of yaw angle, $r$ is the radial station in consideration, $R$ is the rotor radius and $\phi$ is the azimuthal position of the rotor blade. Much of the efforts of the early experiments in yawed flow HAWTs were aimed at understanding the wake expansion and deflection. This enabled various improvements in the classical BEM techniques by improving the parameter $K$ in the Glauert expression for the azimuthally varying induction [see Eq. (19)]. There are various models of the function $K$ some of which are given here.

Coleman et al. [21]:

$$K = tan\left(\frac{\chi}{2}\right) \tag{20}$$

White and Blake [26]:

$$K = \sqrt{2}sin(\chi) \tag{21}$$

Pitts and Peters [27]:

$$K = \frac{15\pi}{32}tan\left(\frac{\chi}{2}\right) \tag{22}$$

Howlett [28]:

$$K = sin^2(\chi) \tag{23}$$

where $\chi$ is the skew angle; the angle between the wake and rotor axis. In the BEM formulation, this angle is defined as follows:

$$tan\chi = \frac{(U_\infty sin\gamma)}{(U_\infty cos\gamma - u_a)} \tag{24}$$

The $K$ factors derived from the different models listed earlier are plotted in **Figure 7** to compare the differences. As can be seen, there are dramatic discrepancies between the results of various authors. Since this function will ultimately affect the varying inductions on the plane, knowledge of the induction field is also necessary to create sound models.
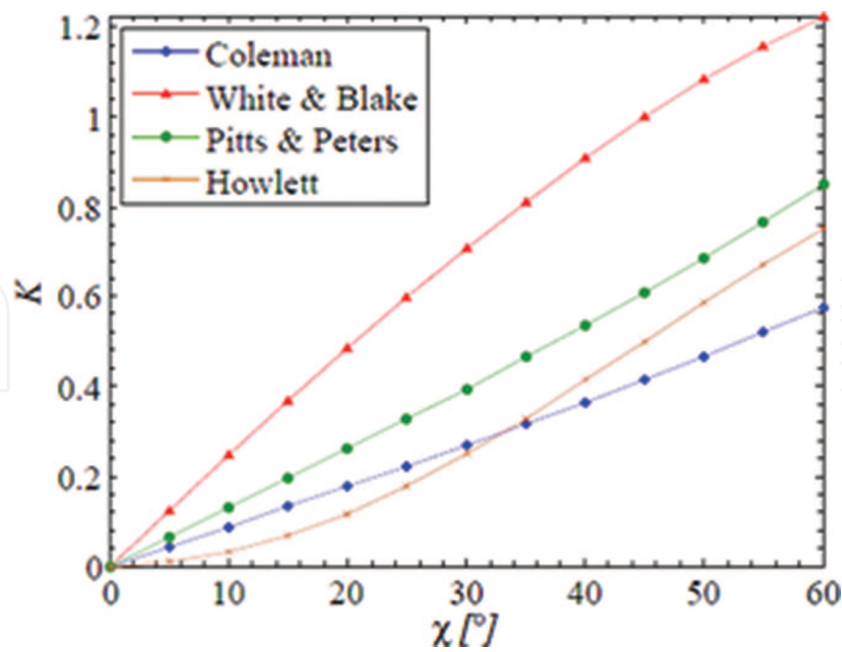
**Figure 7.** Comparison of the variation of K with $\chi$ as predicted by the different models.

Other engineering models were developed in the past years, some of which were examined against measurements in the EU JOULE Dynamic Inflow Projects (see [29, 30]). These models have been implemented in various BEM-based aeroelastic codes. One such model is that developed by Øye [31] and is similar to Glauert's model but introduces a radial variation in induction. The model was derived through a curve fitting procedure with results from an actuator disc model. The induced velocity distribution was found to depend on the radial location, azimuth angle and the wake skew angle:

$$a = a_1\left(1 + f_{2,tudk}\, tan\frac{\chi}{2} sin\, \varnothing\right) \tag{25}$$

$$f_{2,tudk} = \frac{r}{R} + 0.4\left(\frac{r}{R}\right)^3 + 0.4\left(\frac{r}{R}\right)^5 \tag{26}$$

The Glauert correction model [Eq. (19)] gives acceptable results towards the tip region of the blade where the sinusoidal variation of the induction is prevalent. However, the root region of the blade does not exhibit sinusoidal behaviour as was found in the experiments in [32]. Based on this same experiment, Schepers used Fourier series expansions to establish a model for yaw which models better the radial dependency of the induction variation with azimuth (see [33]). This is shown here for a particular radial station along the blade:

$$a = a_1\left(1 - A_1 \cos(\varnothing - \varphi_1) - A_2 \cos(2\varnothing - \varphi_2)\right) \tag{27}$$

where the amplitudes $A_1$ and $A_2$ and the phases $\phi_1$ and $\phi_2$ are curve fitting parameters, all functions of radial position. Also, Ref. [34] (pp. 403–405) recommends the inclusion of higher harmonics in BEM yaw modelling.

### 3.2. Unsteady aerofoil aerodynamics

As discussed earlier, yaw results in an asymmetric flow field where the relative velocity magnitude and direction (and hence angle of attack) both vary with time. Yawed HAWTs are for this reason naturally susceptible unsteady aerodynamic phenomena. Such phenomena give rise to hysteresis effects, even at small angles of attack for which the flow is fully attached. At high angles of attack however, dynamic stall leads to more pronounced hysteresis on both the lift and drag, with the resulting loads often exceeding that static loads significantly. A description of different dynamic stall models applied to wind turbines is presented in [35].

Dynamic stall on a rotating blade is more complex than that experienced in 2D flow conditions. Schreck (see [36, 37]) investigated the 3D dynamic stall processes on the NREL UAE Phase VI rotor through the analysis of blade surface pressure data and the local inflow angle when operating under yawed conditions. In the EU project 'Dynamic stall and 3D effects' coordinated by FFA, it was attempted to use the IEA Annex XVIII measurement to understand dynamic stall effects. An example is given in **Figure 8** for non-yawed conditions in the field. They show measurements of normal force coefficients at 68% span as function of angle of attack (around a low and a high angle of attack) on the Risø experiments, carried out on a 3-bladed, 19 m diameter turbine (see [38]). The angle of attack is derived from a local inflow angle as measured with a pitot probe and corrected for upwash. Hysteresis effects are visible at high angles of attack but in a very disorderly pattern.
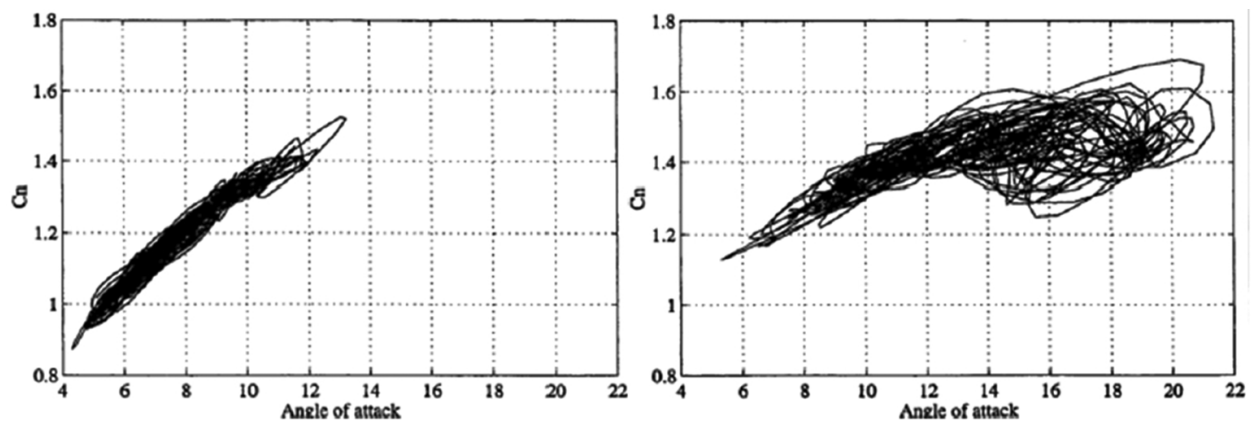


**Figure 8.** Measured normal force coefficient as a function of angle of attack measured at 68% span, low angle of attack series, and high angle of attack series are shown. Source: [38].

The reduced frequency $k$ can be estimated as follows if the freestream velocity is assumed negligible compared to the rotational speed:

$$k = \frac{\Omega c}{2V_{rel}} \approx \frac{\Omega c}{2r\Omega} \approx \frac{c}{2r} \qquad (28)$$

where $c$ is the chord length, $r$ is the radial location along the blade, $\Omega$ is the rotational speed, and $V_{rel}$ is the relative velocity to the blade section. In situations where $k < 0.05$ can be considered steady or quasi-steady, values of $k = 0.1$ are typical for wind turbines in yaw. It is clear that this measure of unsteadiness is a function of the $c/r$ ratio.

In [7], various models are used including a BEM approach (HAWC), an Navier-Stokes solver (EllipSys3D) and an actuator disc solver (HAWC3D) to find the local inflow angle (angle between local relative velocity and chord line) and angle of attack as well as the magnitude of the relative velocity and how it changes. Results are shown for the 91% station on the NREL UAE rotor in **Figure 9**. EllipSys3D results were very accurate as this model includes the effect of the wing geometry in its entirety, and hence, the local inflow angle was calculated. The other results, however, show quite a large difference since the models calculate the actual angle of attack. Despite the differences, the variation of angle of attack with azimuthal position is clear and leads to the unsteadiness that the yawed HAWT suffers from.

Lately, the loads on a yawed wind turbine have been established directly through stereo particle image (SPIV) measurements (see [39]) and reported in [40, 41], but these are limited to only one blade position, thus not allowing for establishing the time variation of the blade loads in yaw.
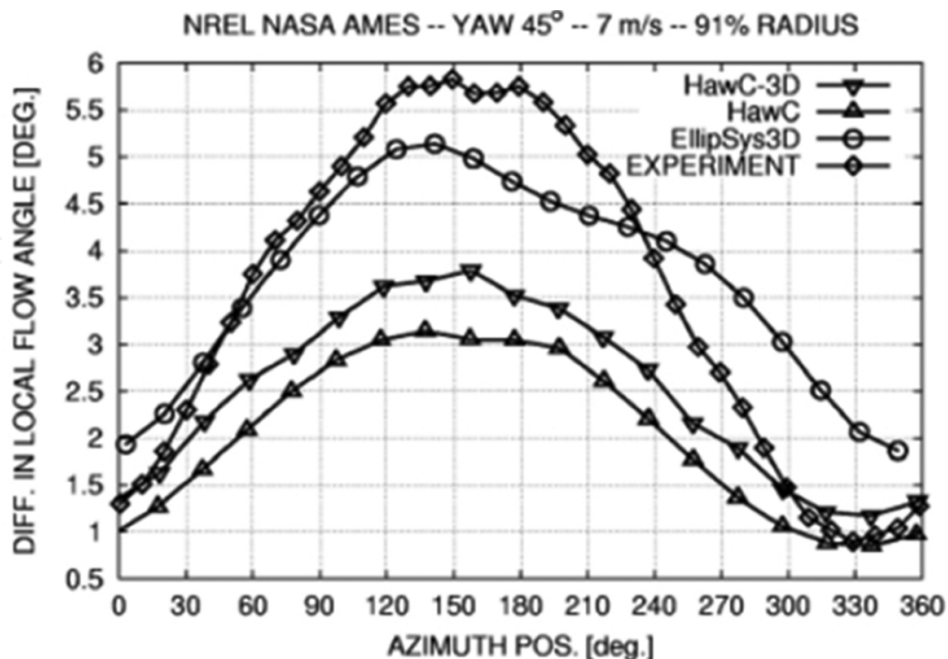


**Figure 9.** Local inflow angle for the NREL UAE rotor at 45° yaw and 7 m/s wind speed. Source: [7].

## 4. Wake characteristics

Experimental research has clearly demonstrated that in reality the wake of a wind turbine is by far more complex than that assumed in the BEM theory. It actually comprises helical vortex sheets, with one sheet originating from each individual rotating blade as illustrated in **Figure 10**. The circulation distribution in the vortex sheet originates from the bound circulation ($\Gamma_B$) developed at the blades. The wake circulation is composed of two vector components: trailing circulation ($\Gamma_T$) that is released from the blades in a direction normal to the trailing edges of the blades and is related to the spanwise variation of bound circulation ($d\Gamma_B/dr$); and shed circulation ($\Gamma_S$) that is released from the blades in a direction parallel to the blades' trailing edges and is related to the variation of bound circulation with time ($d\Gamma_B/dt$). The geometry of the vortex sheet emerging from each individual blade will change such that the edges roll-up (similar to that observed on a wind in linear flight) to form a strong tip vortex and root vortex.
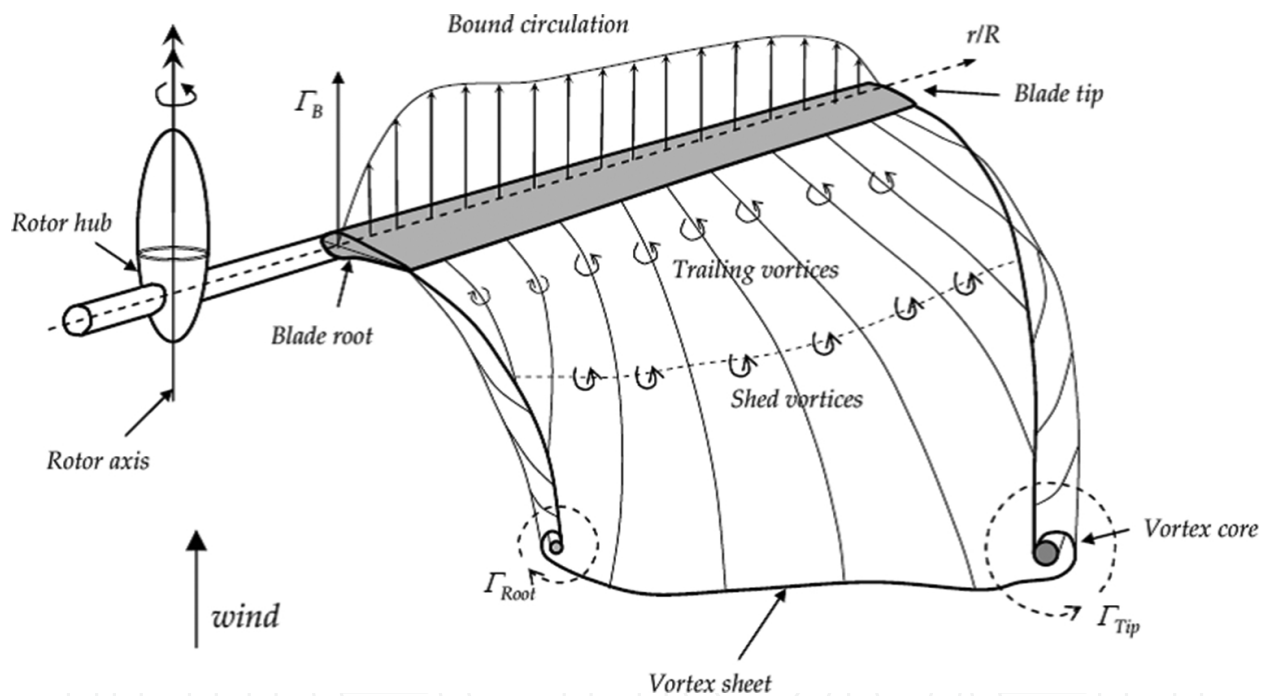


**Figure 10.** The formation of helical vortex sheet by a rotating wind turbine blade. Adapted from [38].

The helical wake of the turbine expands as a consequence of the slowdown of moving air. The higher the operating thrust coefficient, the higher the wake expansion. This has been shown by various researchers such as in [42, 43]. Tip vortices are easily noticeable in experiments on model rotors, even beyond one rotor diameter downstream. Smoke visualizations of tip vortices are shown in **Figure 11**. The root vortices are more difficult to track in experiments and have been only observed much closer to the rotor plane, as, for example, in the recent PIV measurements undertaken [39, 44]. It is most probable that the root vortex diffuses rapidly due to the interference effects of the turbine support structure.

In a yawed rotor, the blade sections have a geometric velocity component in a direction of the free wind speed resulting in the advancing and retreating effect. A variation in both the relative wind speed and angle of attack is experienced with the highest relative velocity reached by the advancing blade when it is vertical pointing upwards. Yawed conditions cause the wake to become skewed leading to an uneven distribution of induction at the rotor disc (see **Figure 12**). Measurements have shown that yawed wind turbines experience a restoring yawing moment. As noted in [23] (pp. 49–53), this moment is not generated by the advancing and retreating blade effect but by the skewed wake geometry which causes the trailing tip vorticity to be on average closer to the downwind side of the rotor plane.



**Figure 11.** Visualisation of the tip vortices for the experiment done under non-yawed conditions by [42].
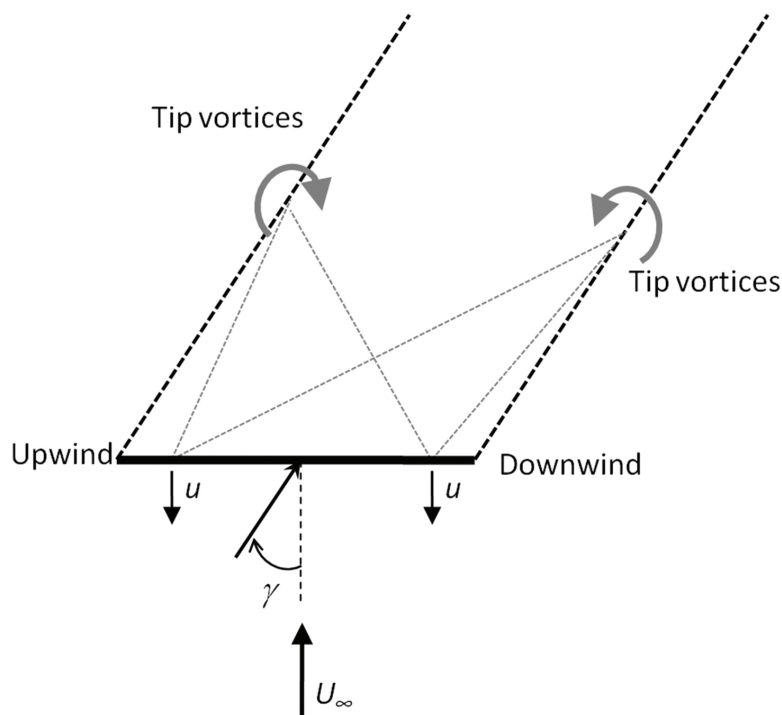


**Figure 12.** Unbalance in the induced velocity from the skewed wake under yawed conditions. Adapted from [23], (pp. 49).

Induced velocities on the upwind side or the rotor are hence lower, leading to large axial thrust loads on the blade sections here to develop a restoring yawing moment.

The influence of the skewed wake geometry on the induction at the rotor plane of yawed turbines was extensively studied in the EU JOULE Dynamic Inflow Projects (refer to Snel and Schepers [29, 30]). The implementation of advanced aerodynamic models based on vortex methods by Voutsinas et al. [45] and the acceleration potential technique by van Bussel [46, 47] has clearly indicated that, in addition to tip vorticity, root vorticity also has a considerable influence on the induction distribution at the rotor plane. However, root vorticity contributes to the generation of a destabilising yawing moment, hence opposing that induced by tip vorticity.

The axial thrust of a rotor with a finite yaw angle varies with azimuth and as a result, the expansion will vary along the azimuthal direction. This has been shown again by Grant et al. [48] and Haans et al. [49]. Some results are shown in **Figure 13**. As can be seen, there is a high expansion in the region where the rotor tip is pointing downwind and almost no expansion in the region where the rotor tip is pointing upwind. These results are coherent with the findings of [48]. The higher the yaw angle, the smaller the thrust coefficient, and hence, the smaller the expansion. Unfortunately, no empirical models have been proposed for the wake deformation in yaw. This would enable practical application in the design of wind turbine blades with applications in BEM or prescribed wake models. Haans et al. [49] have also derived the wake skew angle $\chi$ directly from the smoke visualizations of tip vortices at yaw angles equal to 15°, 30°, and 45°. This angle was found to be larger than the yaw angle at all tested blade pitch angles and tip speed ratios. It was observed that for each tested yaw angle, $\chi$ increased linearly with the measured axial thrust coefficient $C_T$ (see **Figure 14**).

The analysis of wake development requires the use of velocity field measurements over a particular area. Due to this, techniques such as PIV must be used. Such measurements have been performed by [50] and in the MEXICO experiment (see [51]). More recent PIV measurements include those undertaken at TUDelft [39, 52], at NTNU [53] and at Monash University (see [44]). In the experiment by [50], PIV measurements were obtained at various blade azimuthal positions. With these measurements, the variation of the tip vortex circulation was calculated for yaw angles of +30° and -30° yaw as well as for the axial case. **Figure 11** from [50] shows various vorticity contour plots of the tip vortex at various blade azimuth phase angles and at various yaw angles. Information on the magnitude of vorticity is not present so only insight on the iso-vorticity lines can be gained. Soon after release, a 'vorticity tail' becomes apparent from the tip vortex for all cases particularly for yaw. The authors attribute the additional vorticity in these cases to the presence of additional shed vorticity in the wake of a yawed turbine due to the variation of bound vorticity with time. For the -30° yaw, the 'vorticity tail' is first located downstream since the measurement plane is in the upwind direction. For the +30° yaw, the 'vorticity tail' is pointing upwind since the measurement plane is in the downwind direction. As can be noticed, for the +30° yaw case, the vortex remains small. The trailing vorticity from the vortex sheet detaches itself and does not continue to feed into the tip vortex. This is the reason for the low circulation levels found in **Figure 11** of [50]. On the other hand for the -30° yaw case, the interaction between the trailing vorticity and the tip vortex

is more complex and is persistent up to 156° of azimuth blade position. The vortex becomes larger, and the circulation is similar to that found in the axial flow case.
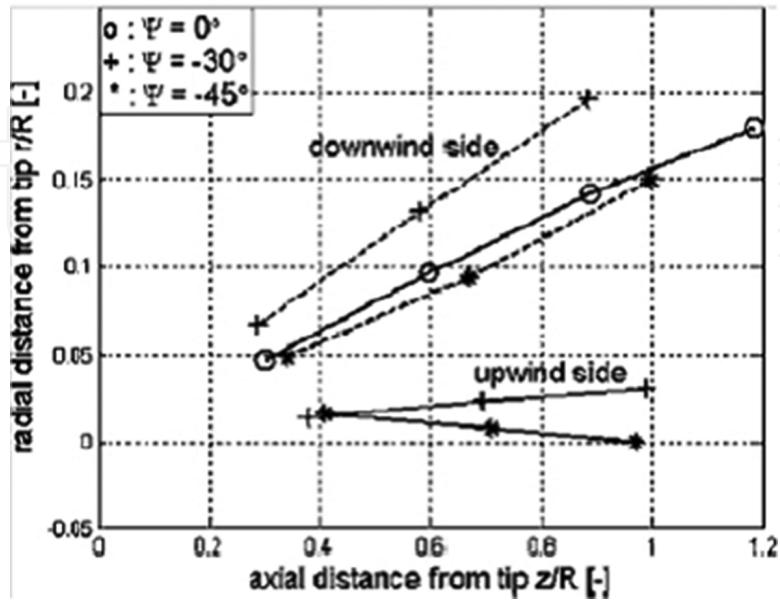


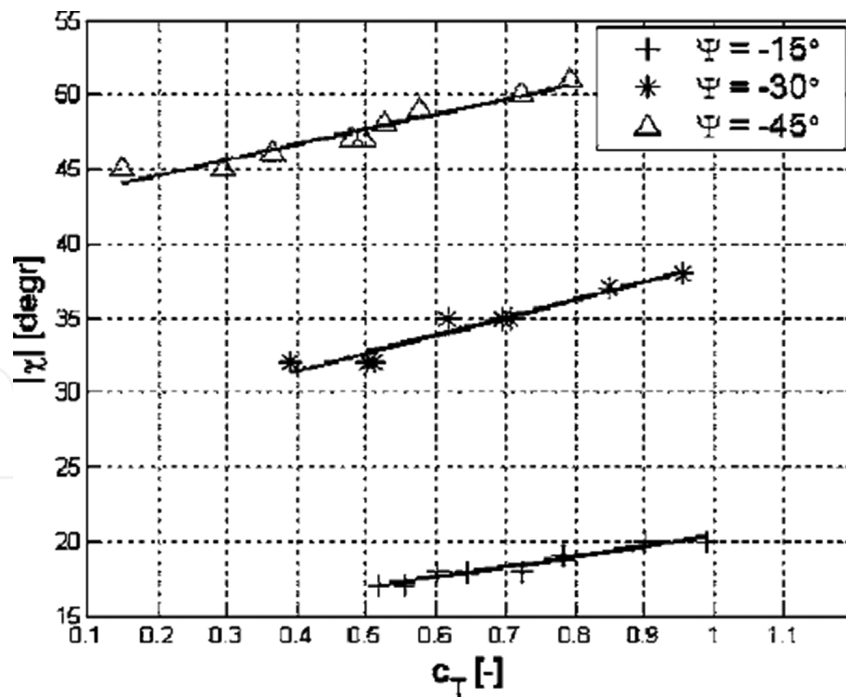**Figure 13.** Wake pitch measurements: Source: [49].



**Figure 14.** $|\chi_s|$ vs $C_T$ for three yawed conditions. Source: [49].

In [54], the authors investigated the radial flows of the MEXICO rotor under both axial and yawed conditions. The investigation was based on both the experimental SPIV measurements

and numerical analysis using a 3D unsteady free-wake vortex model. The study found that the radial velocity increased by a factor of 2 when the turbine was yawed due to the in-plane freestream component. Under axial conditions, it was observed that a slight inboard convection of the tip vortex occurs. This phenomenon was also confirmed later on the more detailed SPIV measurements by Micallef on the TUDelft rotor (see [39]). In these more recent measurements, the tip vortex evolution could be clearly traced as a function of rotor azimuth angle. It could be noted that under yawed conditions, outboard motion of the tip vortex was delayed to a blade azimuth of 10°, even though a radial component equal to $U_\infty \sin\gamma$ was present.

## 5. Summary of research on HAWT rotors in yaw

A comprehensive summary of various experiments on HAWT rotors under both controlled and open field conditions is given in **Table 1**. **Table 2** includes references to various works covering the different aspects of HAWT aerodynamics in yaw discussed in this study.

| Contributor | Year | Type | Rotor diameter | Blade | Variables | Information |
|---|---|---|---|---|---|---|
| Clayton and Filby, University College London | 1982 | HWA in the wake (for averages velocities and turbulence measurements) and power output | 0.5 m (test section size not available) | 3-bladed, no details of the chord, twisted NACA4415, tapered blades | Tip speed ratio, yaw angle, pitch angle | $1.4 \le \lambda \le 9.8$ $0° \le \gamma \le 40°$ $-15° \le \theta \le 15°$ |
| Vestas Tjaereborg 2MW wind turbine | 1983 | Load measurement | 61.1 m | 3-bladed, tapered | N/A | Field experiment |
| NREL UAE Phase I–IV Experiments | 1987 | Blade pressure and load measurements | 10 m | 3-bladed, downwind, Constant chord, Twisted | N/A | Field experiment |
| Vermeer, TUDelft | 1987 | HWA | 2.24 m | 2-bladed, constant chord, twisted, NACA0012 | Yaw angle | Max Re = 2:4e5 |
| Bruining, TUDelft | 1994 | Blade pressure measurements | 10 m | 2-bladed, untapered, untwisted | Tip speed ratio, yaw angle | $4 < \lambda < 10$, $0:5e6 < Re < 1e6$ |
| Grant, Heriot-Watt University | 1997 | Smoke visualization and power output | 0.9 m in open jet tunnel | 2 and 3 blades, tapered | Yaw angle | $\lambda = 6:7$ $5:9e4 < Re < 1e5$ |
| Grant, Heriot-Watt | 2000 | PIV | 0.9 m in open jet tunnel | 3-bladed, tapered, untwisted but pitched, NACA4613, NACA3712 | Yaw angle | $\lambda = 5:2$ $-30° \le \gamma \le 30°$ |

| Contributor | Year | Type | Rotor diameter | Blade | Variables | Information |
|---|---|---|---|---|---|---|
| University | | | | and NACA4611 | | |
| NREL UAE Phase VI Experiment | 2000 | Blade pressure measurements | 10 m in, 4.4 m by 36.6 m wind tunnel | 2-bladed, tapered, twisted, S809 | Tip speed ratio, yaw angle | $1.5 \leq \lambda \leq 7.6$ $0° \leq \gamma \leq 60°$ |
| Medici, KTH Mechanics | 2005 | HWA and load measurement | 0.18 m in 1.2 m by0.8 m wind tunnel | 2-bladed, tapered, untwisted, Gottingen417A | Freestream, tip speed ratio turbulence and yaw angle | $0° \leq \gamma \leq 60°$ $1.2e4 < Re < 3.4e4$ |
| Maeda (field experiment), Mie University | 2005 | Blade pressure measurements and tuft visualization | 10 m | 3-bladed, tapered, twisted, DU and NACA aerofoils | Wind speed and yaw angle | $-45° \leq \gamma \leq 45°$ $3.5e5 < Re < 5.5e5$ |
| Sant and Haans, TUDelft | 2005– 2006 | HWA and smoke visualization | 1.2 m in 2.24 m open-jet tunnel | 2-bladed, constant chord, twisted, NACA0012 | Yaw angle, pitch, tip speed ratio | $-45° \leq \gamma \leq 45°$ $Re \approx 1.7e5$ |
| Maeda (tunnel experiment), Mie University | 2007 | Blade pressure measurements | 2.4 m in 3.6 m open jet tunnel | 3-bladed, tapered, twisted, DU91-W2-250, DU93-W-210 and NACA63-215 | Yaw angle and tip speed ratio | $1.6 \leq \lambda \leq 6.5$ $0° \leq \gamma \leq 45°$ $Re \approx 2.1e5$ |
| MEXICO Experiment | 2007 | Blade pressure measurements and PIV | 4.5 m turbine in 9.5 m by 9.5 m open jet wind tunnel | 3-bladed, tapered, twisted, DUW2-250, RisØ A1-21 and NACA64-418 | Yaw angle, Tip speed ratio, pitch, Parked rotor | $0° \leq \gamma \leq 45°$ and $\gamma = ±45°$ (for PIV) $Re \approx 6.5e5$ |
| Micallef, TUDelft | 2011– 2012 | SPIV measurements | 2 m turbine in octagonal open-jet tunnel of 3 m equivalent diameter | 2-bladed, tapered, twisted, DU96-W180 | Yaw angle and tip speed ratio | $\gamma = 0°$ and $30°$ $\lambda = 5$ (axial flow only) and 7 $Re \approx 3.6e5$ |
| Krogstad and Adaramola, NTNU | 2012 | Power and load measurements, wake measurements using pitot-static probe and LDA | 0.9 m turbine in a wind tunnel test-section 1.9 m by 2.7 m | 3-bladed, tapered, twisted, S826 | Freestream, yaw angle and tip speed ratio | $0° \leq \gamma \leq 50°$ $0.2e5 < Re < 5.0e5$ |

**Table 1.** Overview of experimental campaigns for HAWTs in axial and yawed flow.

| Topic area | Experimental campaigns | Relevant literature |
|---|---|---|
| Gross performance | Clayton and Filby (University College London) Grant (Heriot-Watt University) Sant and Haans (TUDelft) Krogstad and Adaramola (NTNU) | Glauert [25], Clayton and Filby [17], Grant et al. [18], Haans et al. [49], Tongchitpakdee et al. [55], Krogstad et al. [53] |
| Wake geometry and development | Vermeer (TUDelft) Grant (Heriot-Watt University) Sant and Haans (TUDelft) MEXICO experiment Micallef (TUDelft) Krogstad and Adaramola (NTNU) | Øye [31], van Bussell [46, 47], Snel and Schepers [29, 30], Voutsinas et al. [45], Grant et al. [18, 48], Grant and Parkin [50], Hasegawa [56], Schepers [33], Vermeer [32, 43], Vermeer et al. [11], Mikkelsen [56], Haans et al. [49, 57, 58], Sezer-Uzol et al. [59], Schepers and Snel [51], Sant [34], Schepers et al. [23, 60], Sørensen et al. [61], Micallef et al. [52, 54], Micallef [39], Krogstad et al. [53], Sherry et al. [44] |
| Rotor aerodynamics | Bruining (TUDelft) Vermeer (TUDelft) Sant and Haans (TUDelft) Micallef (TUDelft) Krogstad and Adaramola (NTNU) | van Bussell [46, 47], Snel and Schepers [29, 30], Bruining [61], Schepers [23, 33, 60], Mikkelsen [62], Tongchitpakdee et al. [55], Haans et al. [49, 57, 63] Sezer-Uzol et al. [59], Sant [34, 64], Maeda et al. [65], Micallef et al. [52, 53], Micallef [39], Suzuki and Chattot [66], Krogstad et al. [53] |
| Aerofoil aerodynamics | Vestas Tjaereborg 2MW wind turbine Bruining (TUDelft) NREL UAE Phase I–IV Experiment NREL UAE Phase VI Experiment Maeda (Mie University)—field experiment Maeda (Mie University)—wind tunnel experiment MEXICO experiment | Voutsinas et al. [45], Bruining [67], Schreck et al. [36, 37, 68–70], Hand et al. [8], Madsen et al. [7], Johensen et al. [71], Tangler [72], Tongchitpakdee et al. [55], Maeda and Kawabuchi [73], Sezer-Uzol et al. [58], Sant [34], Breton et al. [74], Schmitz and Chattot [75], Shen et al. [76, 77], Schepers et al. [60], Schepers [23], Holierhoek et al. [35] |

**Table 2.** Areas of research in yawed HAWT aerodynamics along with the experimental campaigns available and the relevant literature articles.

# 6. Conclusions and outlook

The fundamental physics of HAWT aerodynamics under yawed conditions has been discussed with reference to some of the latest works. Parallel research on helicopter rotor aerodynamics

has been shown to consist of a wealth of information which can be transposed to wind turbine rotor research. While no Mach number dependence would be expected for a HAWT rotor, the Reynolds number effect on the performance of aerofoils becomes very relevant since the currently available controlled experiments reproduce the rotor model on a much smaller scale.

It is clear that the current trend is towards the understanding of detailed flow fields around the blades. While various researchers have successfully utilized vortex methods and CFD to provide fundamental understanding of the flow, there is still the need for simple physical models which can be used in industry with little computational overhead. While BEM approaches utilize a number of engineering models to refine the representation of the physics, the fundamental assumptions in this theory ignore flow three-dimensionality. A simple approach such as BEM but which takes into account flow three-dimensionality would be very useful especially when dealing with the issue of yaw. More advanced issues such as 3D aerofoil aerodynamics have also been discussed and an overview of the most fundamental research questions which still need to be addressed has been given.

Knowledge of the complex 3D flow phenomena over wind turbine blades in yaw is still limited. New and more reliable models are necessary for modelling 3D aerofoil data to account for the combined effects of stall delay and unsteady flows. Better models are also necessary for modelling aerofoil data at the tip. The undertaking of more experiments under both controlled and open field conditions and with the latest sophisticated measurements techniques remains crucial for deepening the level of knowledge about the flow physics of yawed turbines.

As larger wind turbines rotors are being developed, especially for offshore deployment, rotor aerodynamics will play a more critical role to ensure a successful future for the wind energy industry. The design of larger wind turbine blades presents new challenges for engineers, making it more important to integrate more sophisticated and efficient aerodynamic models in design codes allowing fully coupled multi-physical simulation of entire wind turbine systems to solve complex fluid–structural interaction, control and cost optimisation problems. Further research in yaw aerodynamics should also cater for the latest technology development trends involving larger but more flexible blades and the implementation of smart control algorithms allowing to wind turbines in arrays to be controlled with a coordinated approach to minimise the negative impacts of aerodynamic turbine-to-turbine interactions on the energy yield from large wind farms.

## Author details

Daniel Micallef[1*] and Tonio Sant[2]

*Address all correspondence to: daniel.micallef@um.edu.mt

1 Department of Environmental Design, Faculty for the Built Environment, University of Malta, Malta

2 Department of Mechanical Engineering, Faculty of Engineering, University of Malta, Malta

# References

[1]   Betz A (1919) *Schraubenpropeller mit Geringstem Energieverlust* (Dissertation, Gottingen Nachrichten, Gottingen)

[2]   Dolan, D.S.L. and Lehn, P.W. (2006). Simulation model of wind turbine 3p torque oscillations due to wind shear and tower shadow. In *Power Systems Conference and Exposition, 2006. PSCE '06. 2006 IEEE PES*, Oct. 29 2006–Nov. 1 2006, pp. 2050–2057. doi: 10.1109/PSCE.2006.296240

[3]   Micallef, D., Simao Ferreira, CJ., Sant, T. and Van Bussel, G.J.W. (2010). An analytical model of wake deflection due to shear flow. In *The 3rd EWEA Conference-Torque 2010: The Science of making Torque from Wind*, *Heraklion, Crete, Greece*, 28–30 June 2010.

[4]   Rosen, A. and Sheinman, Y. (1994). The average output power of a wind turbine in a turbulent wind. *Journal of Wind Engineering and Industrial Aerodynamics*, 51(3):287–302. ISSN 0167-6105.

[5]   Wagner, R., Antoniou, I., Pedersen, S.M., Courtney, M.S. and Jørgensen, H.E. (2009). The influence of the wind speed profile on wind turbine performance measurements. *Wind Energy*, 12:348–362. doi:10.1002/we.297

[6]   Eggleston, D.M. and Starcher, K. (1990). A comparative study of the aerodynamics of several wind turbines using flow visualization. *Journal of Solar Energy Engineering*, 112:301–309.

[7]   Madsen, H., Sørensen, N. and Schreck, S. (2003). Yaw aerodynamics analyzed with three codes in comparison with experiment. In *AIAA Paper 2003-519, 41st AIAA Aerospace Sciences Meeting and Exhibit*, Reno, Nevada.

[8]   Hand, M., Simms, D., Fingersh, L., Jager, D., Cotrell, J., Schreck, S. and Larwood, S. (2001). Unsteady aerodynamics experiment phase VI: Wind tunnel test configurations and available data campaigns. Technical Report NREL/TP-500-29955, National Renewable Energy Laboratory, Colorado.

[9]   Akay, B., Micallef, D., Simão Ferreira, C.J. and van Bussel, G.J.W. (2014). Effects of geometry and tip speed ratio on the HAWT blade's root flow. Journal of Physics: Conference Series 555 (2014) 012002; doi:10.1088/1742-6596/555/1/012002.

[10]  Micallef, D., Ferreira, C.S., Sant, T., and Bussel, G.J.W. (2015). Experimental and numerical investigation of tip vortex generation and evolution on horizontal axis wind turbines. *Wind Energy.* doi:10.1002/we.1932

[11]  Vermeer, L.J., Sørensen, J.N. and Crespo, A. (2003). Wind turbine wake aerodynamics. *Progress in Aerospace Sciences*, 98:467–510.

[12]  Wang, T. (2012). A brief review on wind turbine aerodynamics. *Theoretical and Applied Mechanics Letters*, 2(6). Article 062001, ISSN 2095-0349.

[13] Leishman, J.G. (2002). Challenges in modeling the unsteady aerodynamics of wind turbines. *Wind Energy*, 5(11):85–132.

[14] Barthelmie, R., Frandsen, S., Rathmann, O., Hansen, K., Politis, E., Prospathopoulos, J., Schepers, J., Rados, K., Cabezon, D., Schlez, W., Neubert, A. and Heath, M. (2011). Flow and wakes in large wind farms: Final report for UpWind WP8. Technical Report Risø-R-1765(EN), Risø DTU, National Laboratory for Sustainable Energy.

[15] Hansen, M.O.L. and Johansen, J. (2004). Tip studies using CFD and comparison with tip loss models. *Wind Energy*, 7(4), October/December 2004, pp. 343–356.

[16] Anderson, M. (1979). Horizontal wind turbine in yaw. In *Proc. 1st BWEA Wind Energy Conference*, Cranfield University of Technology, pp. 68–77.

[17] Clayton, B. and Filby, P. (1982). Measured effects of oblique flows and change in blade pitch angle on performance and wake development of model wind turbines. In *Proc 4th BWEA Wind Energy Conference*, Cranfield Institute of Technology, UK.

[18] Grant, I., Parkin, P. and Wang, X. (1997). Optical vortex tracking of a horizontal axis wind turbine in yaw using laser-sheet, flow visualisation. *Experiments in Fluids*, 23(6): 513–519.

[19] Hansen, M. (2008). *Aerodynamics of Wind Turbines*, second edition. Earthscan., UK pp. 45–62.

[20] Glauert, H. (1926a). *The Analysis of Experimental Results in the Windmill Brake and Vortex Ring States of an Airscrew*. ARCR R&M 1026, Aeronautical Research Council (ARS), UK.

[21] Coleman, R., Feingold, A. and Stempin C.W. (1945). *Evaluation of the Induced Velocity Fields of an Idealized Helicopter Rotor*. NACA ARR L5E10, National Advisory Committee for Aeronautics (NACA), USA.

[22] Schepers, J.G. and Schreck, S. (2013). The importance of aerodynamics and the role of aerodynamic measurements, ECN-M-13-002, Energy Research Centre of the Netherlands. *Presented at the Science of Making Torque from Wind Conference*, Olderburg, Germany, 2012.

[23] Schepers, J.G. (2012). Engineering models in wind energy aerodynamics—Development, implementation and analysis using dedicated aerodynamic measurements. PhD thesis, Delft University of Technology. Available online from http://repository.tudelft.nl

[24] Burton, T., Sharpe, D., Jenkins, N. and Bossanyi, E. (2011). *Wind Energy Handbook.* John Wiley & Sons Ltd., West Sussex, UK. pp. 139–141.

[25] Glauert, H. (1926b). *A General Theory of the Autogyro*. ARCR R and M 1111, Aeronautical Research Council (ARS), UK.

[26] White, F. and Blake, B. (1979). Improved method of predicting helicopter control response and gust sensitivity. In *Proceedings of the 35th Annual Forum of the American Helicopter Soc.*, Washington, DC.

[27] Pitts, D. and Peters, D. (1981).Theoretical prediction of dynamic inflow derivatives. *Vertica*, 5:21–34.

[28] Howlett, J. (1981). *UH-60A Blackhawk Engineering Simulation Program: Vol 1: Mathematical Model*. NASA CR-66309, National Aeronautics and Space Administration (NASA), USA.

[29] Snel, H. and Schepers, J.G. (Ed.) (1994). *Joint Investigation of Dynamic Inflow Effects and Implementation of an Engineering Method*. Energy Research Centre of the Netherlands, Petten, the Netherlands, ECN-C-94-107.

[30] Snel H. and Schepers J.G. (Ed.) (1995). *Dynamic Inflow: Yawed Conditions and Partial Span Pitch Control*. Energy Research Centre of the Netherlands, Petten, the Netherlands, ECN-C-95-056.

[31] Øye, S. (1992). Induced velocities for rotors in yaw. In *Proceedings of the Sixth IEA Symposium*, ECN, Petten, The Netherlands.

[32] Vermeer, L. (1998). Wind tunnel experiments on a rotor model in yaw. In *Proceedings of the 12th symposium on Aerodynamics of Wind Turbines*, Lyngby, Denmark.

[33] Schepers, J. (1999). An engineering model for yawed conditions, developed on basis of wind tunnel measurements. In *Proceedings of the 37th Aerospace Sciences Meeting and Exhibit, AIAA-1999-39*, Reno, NV, USA.

[34] Sant, T. (2007). Improving BEM-based aerodynamics models in wind turbines design codes. PhD thesis, Delft University of Technology. Available online from http://www.tudelft.nl

[35] Holierhoek, de Vaal, J.B., van Zuijlen, A.H. and Bijl, H. (2013). Comparing different dynamic stall models. *Wind Energy*, 16(1):139–158.

[36] Schreck, S., Robinson, M., Hand, M. and Simms, D. (2000). HAWT dynamic stall response asymmetries under yawed flow conditions. In *Proceedings of the 36th ASME/AIAA Wind Energy Symposium*, Reno, Nevada.

[37] Schreck, S., Robinson, M., Hand, M. and Simms, D. (2001). Blade dynamic stall vortex kinematics for a horizontal axis wind turbine in yawed conditions. *Journal of Solar Energy Engineering*, 123(4):272–281.

[38] Schepers, J., Brand, A., Madsen, H., Stefanatos, N., Simms, D., Hand, M., Bruining, A., van Rooij, R., Shimizu, Y., Maeda, T. and Graham, M. (2001). IEA annex xiv/xviii, field rotor aerodynamics. In *Proceedings of the EWEC Conference*, Brussels.

[39] Micallef, D (2012c). 3D flows near a HAWT rotor: A dissection of blade and wake contributions. PhD Thesis, Delft University of Technology.

[40] del Campo, V., Ragni, D., Micallef, D., Akay, B., Diez, F.J. and Simão Ferreira, C.J. (2014). 3D load estimation on a horizontal axis wind turbine using SPIV. *Wind Energy*, 17:1645–1657. doi:10.1002/we.1658

[41] del Campo, V., Ragni, D., Micallef, D., Diez, F.J. and Ferreira, C.J.S. (2015). Estimation of loads on a horizontal axis wind turbine operating in yawed flow conditions. *Wind Energy*, 18:1875–1891. doi:10.1002/we.1794

[42] Alfredsson, P.-H. and Dahlberg, J.-A. (1981). *A Preliminary Wind Tunnel Study of Windmill Wake Dispersion in Various Flow Conditions*, The Aeronautical Research Institute of Sweden (FFA), Sweden. Technical Note AU-1499, Part 5.

[43] Vermeer, L. (2001). A review of wind turbine wake research at TUDELFT. In *A Collection of the 2001 ASME Wind Energy Symposium Technical Papers*, USA pp. 103–113.

[44] Sherry, M., Sheridan, J. and Jacono, D.L. (2013). Characterisation of a horizontal axis wind Turbine's tip and root vortices. *Journal Experiments in Fluids,* 54:1417.

[45] Voutsinas, S.G., Belessis, M.A. and Rados K.G. (1995). Investigation of the yawed operation of wind turbines by means of a vortex particle method. *AGARD-CP-552 FDP Symposium on Aerodynamics and Aeroacoustics of Rotorcraft*, Berlin, Germany.

[46] vanBussel, G. (1993). *The Acceleration Potential Models PREDICHAT/PREDICDYN Applied for Calculation of Axisymmetric Dynamic Inflow Cases, IW-93071R*, Delft University of Technology, the Neterlands.

[47] vanBussel, G. (1995). The aerodynamics of horizontal axis wind turbine rotors explored with asymptotic expansion methods. PhD thesis, Technische Universiteit Delft.

[48] Grant, I., Mo, M., Pan, X., Parkin, P., Powell, J., Reinecke, H., Shuang, K., Coton, F. and Lee, D. (2000). An experimental and numerical study of the vortex filaments in the wake of an operational, horizontal-axis, wind turbine. *Journal of Wind Engineering and Industrial Aerodynamics*, 23(6):513–519.

[49] Haans, W., Sant, T., van Kuik, G., and van Bussel, G. (2005). Measurement of tip vortex paths in the wake of a HAWT under yawed flow conditions. *Journal of Solar Energy Engineering*, 127(4):456–463.

[50] Grant, I. and Parkin, P. (1999). A DPIV study of the trailing vortex elements from the blades of a horizontal axis wind turbine in yaw. *Experiments in Fluids*, 28:368–376.

[51] Schepers, J.G. and Snel, H. (2007). *Model Experiments in Controlled Conditions (MEXICO)*, Energy Research Centre of the Netherlands, Petten, the Netherlands. ECN-E-07-042.

[52] Micallef, D., van Bussel, G.J.W., Ferriera, C.S. and Sant, T. (2012a). The origins of a wind turbine tip vortex. In *Proceedings from the Science of making Torque from Wind Conference*, Olderburg, Germany.

[53]   Krogstad, P.Å. and Adaramola, M.S. (2012). Performance and near wake measurements of a model horizontal axis wind turbine. *Wind Energy*, 15(5):743–756.

[54]   Micallef, D., van Bussel, G.J.W., Ferriera, C.S. and Sant, T. (2012b). An investigation of radial velocities for a horizontal axis wind turbine in axial and yawed flows. *Wind Energy*, 16(4):529–544.

[55]   Tongchitpakdee, C., Benjanirat, S. and Sankar, L.N. (2005). Numerical simulation of the aerodynamics of horizontal axis wind turbines under yawed flow conditions. *Journal of Solar Energy Engineering*, 127(4):464–474.

[56]   Hasegawa, Y. (1999). Numerical analysis of yawed inflow effects on a HAWT rotor. In *Proc. of 3rd ASME/JSME Joint Fluids Eng. Conf.*, FEDSM99-7820.

[57]   Haans, W., Sant, T., van Kuik, G. and van Bussel, G. (2008). HAWT near wake aerodynamics, part I: axial flow conditions. *Wind Energy*, 11(3):19.

[58]   Haans, W. (2011). Wind turbine aerodynamics in yaw, unravelling the measured rotorwake. PhD Thesis, Delft University of Technology. Available online from http://repository.tudelft.nl

[59]   Sezer-Uzol, N. and Long, L.N. (2006). AIAA Paper 2006-0394. *Presented at AIAA Aerospace Sciences Meeting*, Reno, NV.

[60]   Schepers, J.G., Boorsma, K., et al. (2011). *Final Report of IEA Task 29, Mexnext (Phase 1), Analysis of Mexico Wind Tunnel Measurements*. ECN-E-12-004, Energy Research Center of the Netherlands, ECN.

[61]   Sørensen, N.N., Bechmann, A., Réthoré, P.-E. and Zahle, F. (2012). Near wake Reynolds-averaged Navier–Stokes predictions of the wake behind the MEXICO rotor in axial and yawed flow conditions. *Wind Energy.*, 17(1), 2014, p. 75–86. doi:10.1002/we.155

[62]   Mikkelsen, R. (2003). Actuator disc methods applied to wind turbines. PhD thesis, Technical University of Denmark, Lyngby, Denmark.

[63]   Haans, W., van Kuik, G. and van Bussel, G. (2007). Experimentally observed effects of yaw misalignment on the inflow in the rotor plane. *Journal of Physics: Conference Series*, 75:10.

[64]   Sant, T., van Bussel, G. and van Kuik, G. (2009). Estimating the angle of attack from blade pressure measurements on the NREL Phase VI using a free wake vortex model: Yawed conditions. *Wind Energy*, 12:1–32.

[65]   Maeda, T., Kamada, Y., Suzuki, J. and Fujioka, H. (2008). Rotor blade sectional performance under yawed inflow conditions. *Journal of Solar Energy Engineering*, 130:031018-1–031018-7.

[66]   Suzuki, K. and Chattot, J.J. (2012). Unsteady hybrid Navier–Stokes/vortex model applied to wind turbine aerodynamics under yaw conditions. In *Proceedings from the*

*Seventh International Conference on Computational Fluid Dynamics (ICCFD7)*, Big Island, Hawaii.

[67] Bruining, W. (1997). Aerodynamic characteristics of a 10 m diameter rotating wind turbine blade experimental results from the Delft University of Technology for the "Dynamic Stall and 3D Effects Project". IW95-084R, TU Delft, Institute of Wind Energy.

[68] Shreck, S. and Robinson, M. (2002). Rotational augmentation of horizontal axis wind turbine blade aerodynamic response. *Wind Energy Special Issue: Analysis and Modeling of the NREL Full-Scale Wind Tunnel Experiment*, 5(2–3):133–150.

[69] Schreck, S. and Robinson, M. (2005). Blade three-dimensional dynamic stall response to wind turbine operating condition. *Journal of Solar Energy Engineering*, 127(4):488–495.

[70] Schreck, S., Sant, T. and Micallef, D. (2010). Rotational augmentation disparities in MEXICO and UAE phase VI experiments. In *Proceedings from the Conference Science of Making Torque from Wind, Organised by the European Academy of Wind Energy*, Crete.

[71] Johansen, J. and Sørensen, N.N. (2004). Aerofoil characteristics from 3D CFD rotor computations. *Wind Energy*, 7(4):283–294.

[72] Tangler, J.L. (2004). Insight into wind turbine stall and post-stall aerodynamics. *Wind Energy*, 7(3):247–260.

[73] Maeda, T. and Kawabuchi, H. (2005). Surface pressure measurement on a rotating blade of field horizontal axis wind turbine in yawed conditions. *JSME International Journal*, 48:156–163.

[74] Breton, S.P., Coton, F.N. and Moe, G. (2008). A study on rotational effects and different stall delay models using a prescribed wake vortex scheme and NREL phase VI experiment data. *Wind Energy*, 11(5):459–482.

[75] Schmitz, S. and Chattot, J. (2009). Flow physics and stokes theorem in wind turbine aerodynamics. *Computational Fluid Dynamics*, 9:801–806.

[76] Shen W.Z., Hansen, M. and Sørensen, J. (2008). Determination of the angle of attack on rotor blades. *Wind Energy*, 12(1):91–98.

[77] Shen, W.Z., Hansen, M.O.L. and Sørensen, J.N. (2009). Determination of the angle of attack on rotor blades. *Wind Energy*, 12(1):91–98.